

# The complex structure of hyperionization regions of the Oe star HD 175754

E. Danezis, A. Antoniou, E. Lyratzi, E. Theodossiou, M. Stathopoulou,  
D. Nikolaidis, C. Drakopoulos, A. Soulikias & M. Koutroumanou

University of Athens, School of Physics  
Department of Astrophysics, Astronomy and Mechanics  
Panepistimiopolis, Zografos 157 84  
Athens – Greece

## Abstract

In this paper we present a study of the UV resonance lines SiIV, CIV, NV and the NIV line ( $\lambda$  1718.80 Å) of the Oe star HD 175754, using 7 spectrograms, taken by IUE, between September 1978 and August 1981. We reproduced the above mentioned lines by the model proposed by Danezis et al. (2003), which is based on the idea of independent density layers in the regions where the spectral lines that present SACs (DACs) are created. We calculated the apparent rotation ( $V_{rot}$ ) and expansion/contraction velocities ( $V_{exp}$ ) of these density regions, as well as their  $\xi$  value, which is an expression of the optical depth. We also present the relation among these parameters and their evolution with time.

## Introduction

HD 175754 is a luminous supergiant star of spectral type OeIf with effective temperature  $T_{eff}=31800 \pm 1100$  °K (Morossi & Crivellari, 1980). Costero & Stalio (1981) and Costero et al (1981) studied the NV, SiIV and CIV profiles of this star and compared them with the profiles of similar type stars' spectra. They found individuality, which implies different structures and dynamics of the atmospheric layers above the photosphere. Carrasco et al. (1981) reported only small changes in the UV resonance line profiles. They interpreted them in terms of variations in dynamics and density/ionization structure of the stellar wind. Lamers et al (1982) noted the possibility of the presence of satellite components superimposed on the wide P Cygni profiles of the UV resonance lines. Finally, Franco et al (1983) studied the P Cygni profiles of the above resonance lines of HD 175754 observed at different epochs and they reported variability at the secondary satellite component. They proposed two different mechanisms for the explanation of the variability, namely, a thermal mechanism in a hot region at  $T_c=2 \times 10^5$  K which produces the principal stationary component and a mechanism which gives rise to the secondary component by ionization of cooler high velocity stellar material from X-rays coming from inner coronal region.

In this paper we present the study of the superionized regions in the gaseous envelope of HD 175754 (Lamers et al. 1982 and Franco et al. 1983), based on the proposed by Danezis et al. (2003) model for the structure of the SACs regions in the early type atmospheres. This model presupposes that the regions, where these spectral lines are formed, are not continuous but consist of a number of independent absorbing density layers of matter, followed by an emission region and an external general absorption region. By this model, we calculate the apparent expansion/contraction velocities ( $V_{exp}$ ), the apparent rotation velocities ( $V_{rot}$ ), as well as an expression of the

optical depth ( $\xi$ ), for all the independent density regions of the superionized regions in the gaseous envelope of HD 175754. Finally, we calculate the variations of the above mentioned parameters, in the time period between 1978 and 1981.

### The model: Mathematical expression

Considering an area of gas consisting of  $i$  independent absorbing shells followed by a shell that both absorbs and emits and an outer shell of general absorption, we conclude to the function:

$$I_I = \left[ I_{I_0} \prod_i \exp\{-L_i x_i\} + S_{I_e} (1 - \exp\{-L_e x_e\}) \right] \exp\{-L_g x_g\}$$

where:  $I_{\lambda_0}$ : the initial radiation intensity,

$L_i$ ,  $L_e$ ,  $L_g$ : are the distribution functions of the absorption coefficients  $k_{\lambda i}$ ,  $k_{\lambda e}$ ,  $k_{\lambda g}$  respectively. Each  $L$  depends on the values of the apparent rotation velocity as well as of the radial expansion/contraction velocity of the density shell, which forms the spectral line ( $V_{rot}$ ,  $V_{exp}$ ),

$x = \int_0^s \Omega r ds$  is an expression of the optical depth  $\tau$ , where  $\Omega$ : an expression of

$k_\lambda$  and has the same units as  $k_\lambda$ ,

$S_{\lambda e}$ : the source function, which, at the moment when the spectrum is taken, is constant and

$$L = \sqrt{1 - \cos^2 q_0} \text{ if } \cos q_0 < 1 \text{ and } L = 0 \text{ if } \cos q_0 \geq 1,$$

where  $\cos q_0 = \frac{-I_0 + \sqrt{I_0^2 + 4\Delta I^2}}{2\Delta I z_0}$ , where  $2\theta_0$  is the angular width of the

equatorial disk of matter,  $\lambda_0$  is the wavelength of the center of the spectral line and  $I_0 = I_{lab} + \Delta I_{exp}$ , with  $\lambda_{lab}$  being the laboratory wavelength of the spectral line produced by a particular ion and  $\Delta\lambda_{exp}$  the radial Doppler shift and

$$\frac{\Delta I_{exp}}{I_{lab}} = \frac{V_{exp}}{c}.$$

$z_0 = \frac{V_{rot}}{c}$ , where  $V_{rot}$  is the apparent rotation velocity of the  $i$  density shell of matter and

$\Delta I = |I_i - I_0|$ , where the values of  $\lambda_i$  are taken in the wavelength range we want to reproduce.

The spectral line's profile, which is formed by the  $i$  density shell of matter, must be accurately reproduced by the function  $e^{-L_i x_i}$  by applying the appropriate values of  $V_{roti}$ ,  $V_{expi}$  and  $\xi_i$ . Using the best model's fit for a complex spectral line, we can calculate the apparent expansion/contraction ( $V_{expi}$ ) velocity, the apparent rotation velocity ( $V_{roti}$ ) and an expression of the optical depth ( $\xi_i$ ) of the region in which the main spectral line and its SACs are created.

At this point we would like to point out that the calculated values of the apparent rotation and expansion/contraction velocities correspond to the regions, where the Satellite Absorption Components (SACs) are created, and not to the star.

Specifically, these values correspond to the density regions (blobs, puffs, bubbles) which result when streams of matter are twisted and form strings that produce blobs, puffs or bubbles.

## Data

The data we used are the 7 IUE spectra of HD 175754 taken by the Villafranca Satellite Tracking Station of the European Space Agency (VILSPA) database. Our data are presented in table 1.

Table 1	
Camera	Date
Swp 02813	30/09/1978
Swp 04901	09/04/1979
Swp 06269	23/08/1979
Swp 09320	20/06/1980
Swp 13591	27/03/1981
Swp 13728	16/04/1981
Swp 14803	24/08/1981

In these spectra we studied the structure of the spectral lines SiIV  $\lambda\lambda$  1393.755 Å, 1402.77 Å, CIV  $\lambda\lambda$  1548.185 Å, 1550.774 Å, NIV  $\lambda$  1718.551 Å and NV  $\lambda\lambda$  1238.821 Å, 1242.804 Å.

## Figures

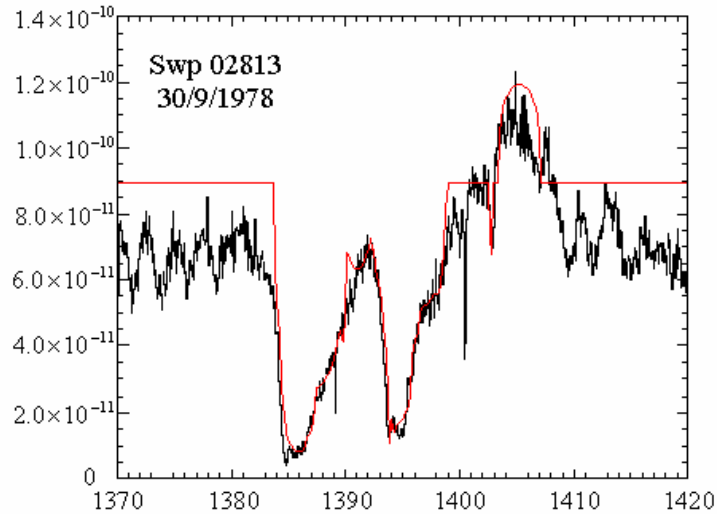


**Figure 1:** Best fit of the SiIV  $\lambda\lambda$  1393.755, 1402.77 Å resonance lines

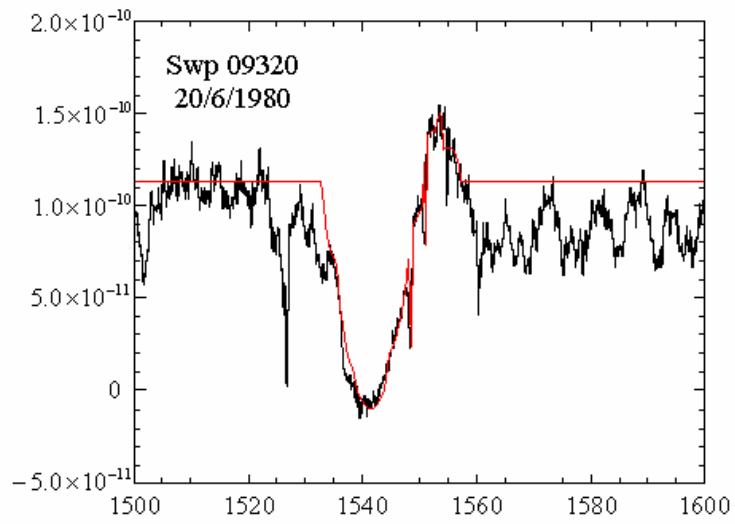


**Figure 2:** Best fit of the CIV  $\lambda$  1548.185, 1550.774 Å resonance lines

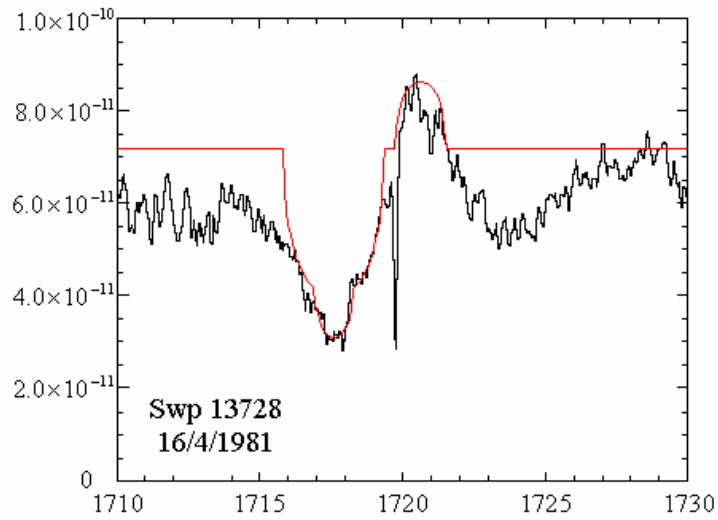


**Figure 3:** Best fit of the NIV  $\lambda$  1718.551 Å line

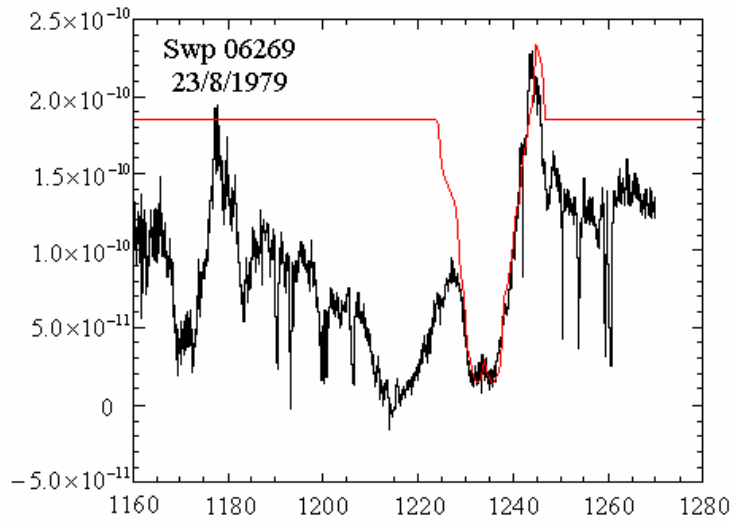


**Figure 4:** Best fit of the NV  $\lambda\lambda$  1238.821, 1242.804 Å resonance lines

### Diagrams and Conclusions

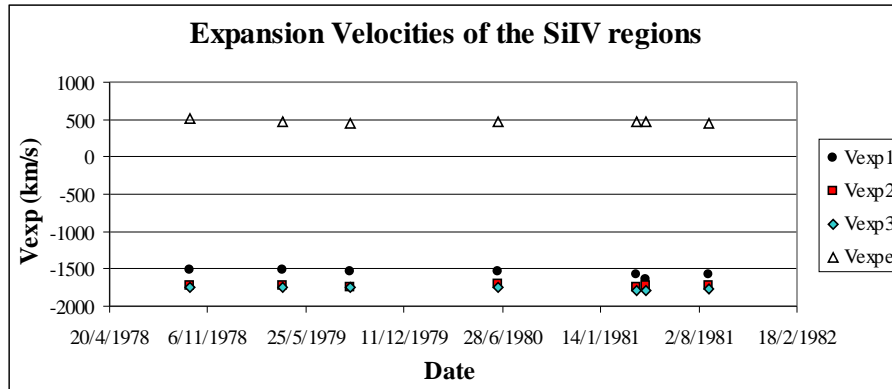


**Diagram 1:** Apparent radial velocities (expansion/contraction) of the three absorption components (SACs) and the emission component of the SiIV doublet as a function of the date. One can see that all the components present almost constant radial velocities with time.

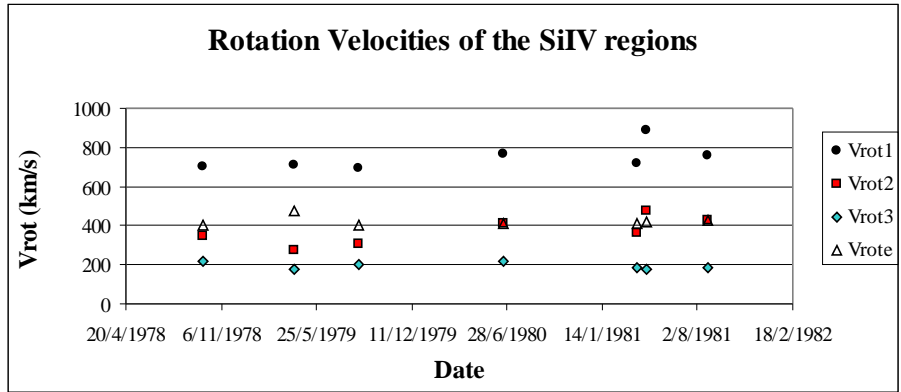


**Diagram 2:** Apparent rotation velocities of the three absorption components (SACs) and the emission component of the SiIV doublet as a function of the date. One can see that all the components present almost constant rotation velocities with time.

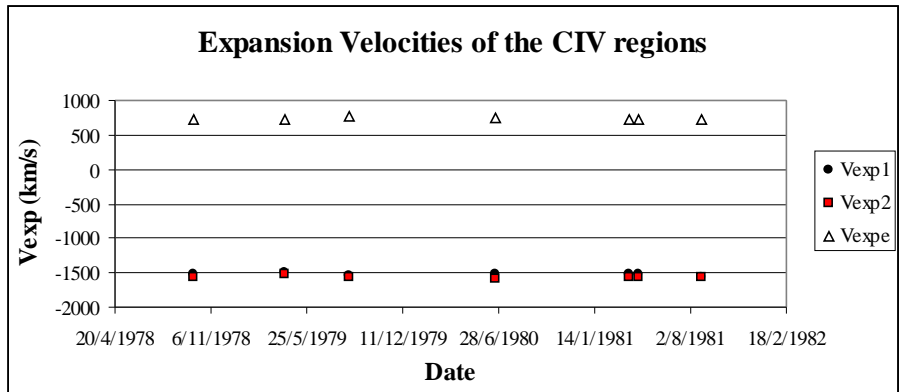


**Diagram 3:** Apparent radial velocities (expansion/contraction) of the two absorption components (SACs) and the emission component of the CIV doublet as a function of the date. One can see that all the components present almost constant radial velocities with time.

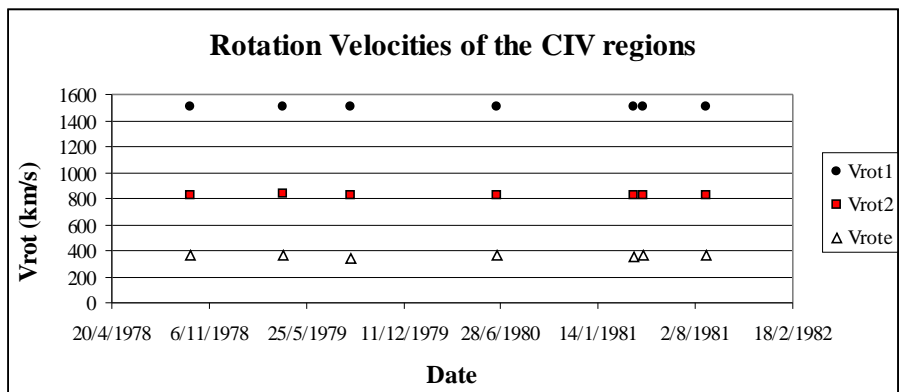


**Diagram 4:** Apparent rotation velocities of the two absorption components (SACs) and the emission component of the CIV doublet as a function of the date. One can see that all the components present almost constant rotation velocities with time.

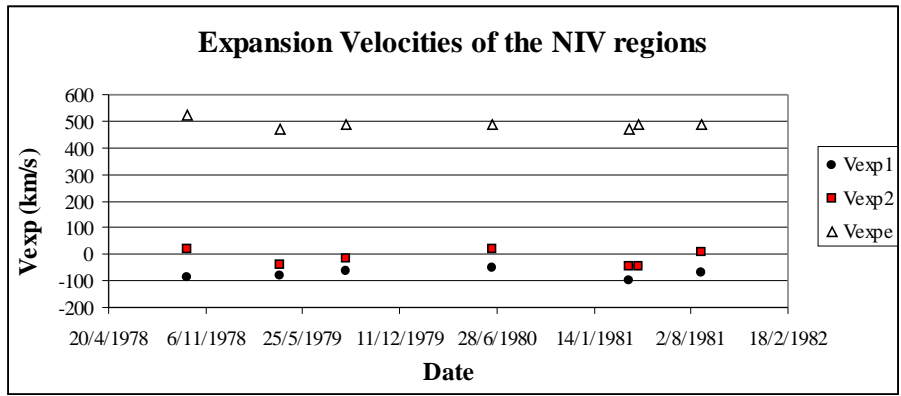


**Diagram 5:** Apparent radial velocities (expansion/contraction) of the two absorption components (SACs) and the emission component of the NIV line as a function of the date. One can see that all the components present almost constant radial velocities with time.

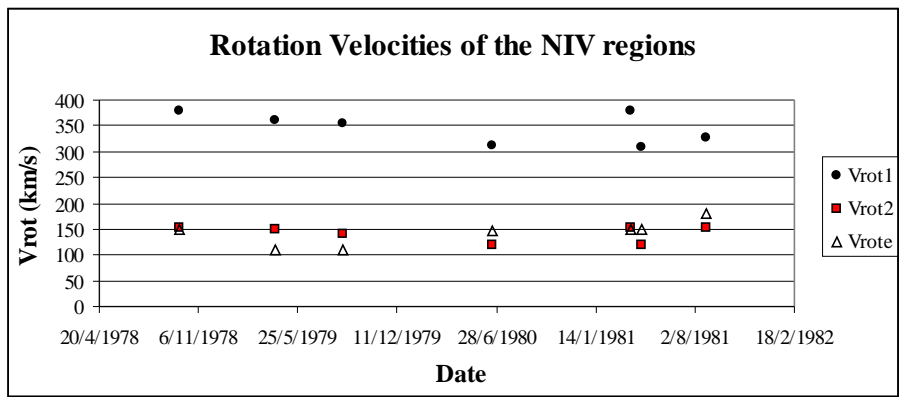


**Diagram 6:** Apparent rotation velocities of the two absorption components (SACs) and the emission component of the NIV line as a function of the date. One can see that all the components present almost constant rotation velocities with time.

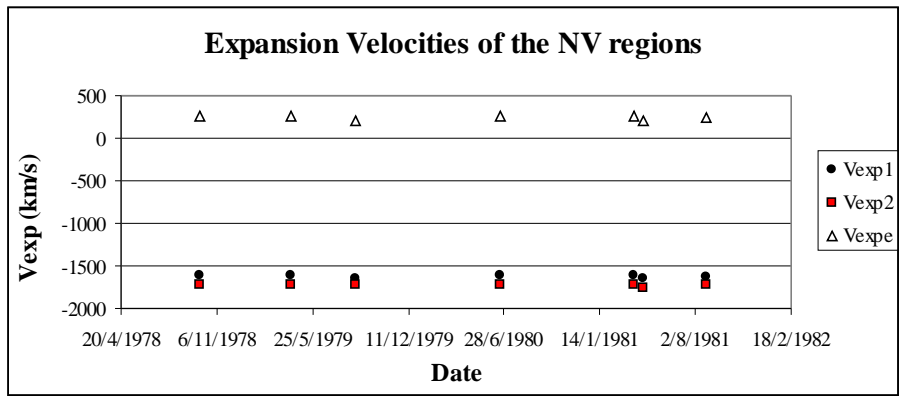


**Diagram 7:** Apparent radial velocities (expansion/contraction) of the two absorption components (SACs) and the emission component of the NV doublet as a function of the date. One can see that all the components present almost constant radial velocities with time.

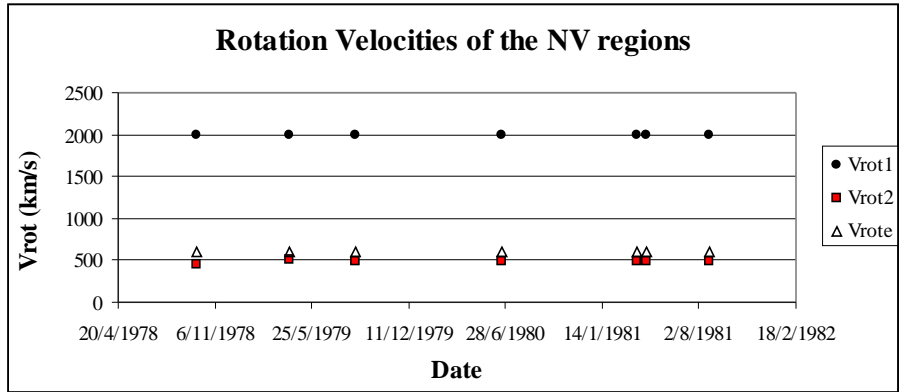


**Diagram 8:** Apparent rotation velocities of the two absorption components (SACs) and the emission component of the NV doublet as a function of the date. One can see that all the components present almost constant rotation velocities with time.

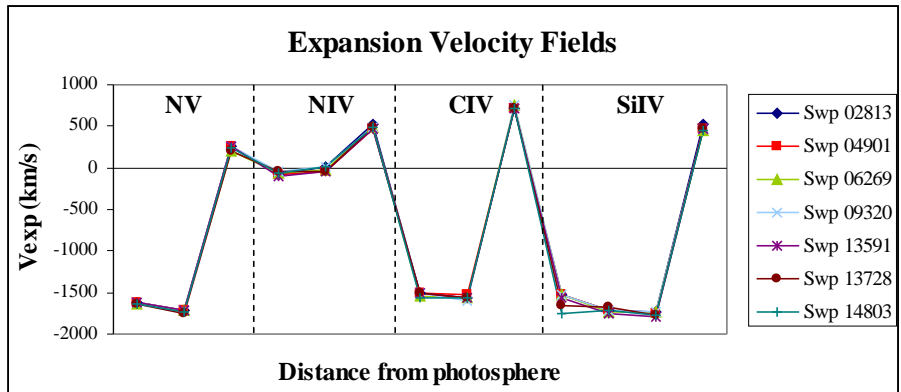


**Diagram 9:** Apparent radial velocity fields for all the studied spectra. It is clearly seen that all the studied atmospherical regions present radial velocities that remain almost constant with time in the period from September 1978 to August 1981.

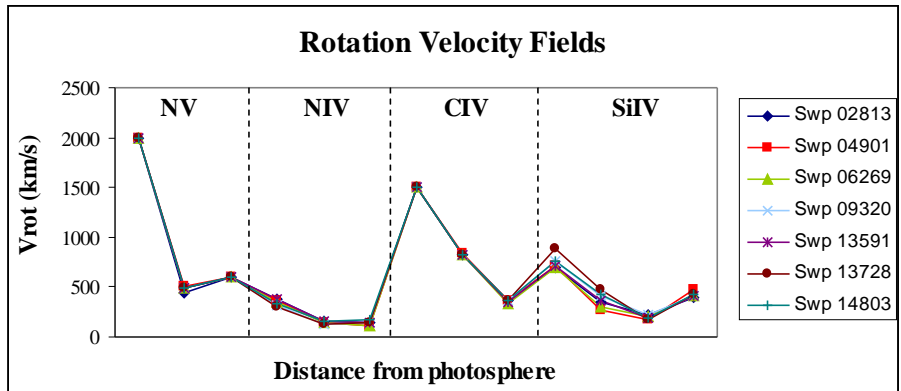


**Diagram 10:** Apparent radial velocity fields for all the studied spectra. As in the case of the radial velocities, also the rotation velocities of the studied atmospherical regions remain almost constant with time in the period from September 1978 to August 1981.

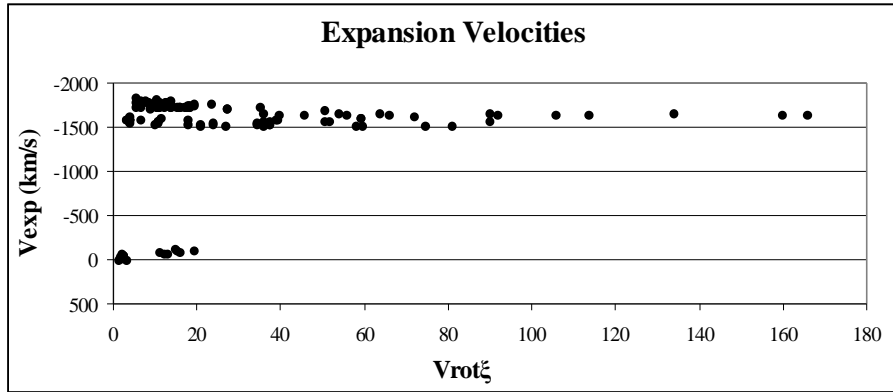


**Diagram 11:** Apparent radial velocities ( $V_{\text{exp}}$ ) as a function of an expression of the absorbed energy ( $V_{\text{rot}}\xi$ ), for all the ions and all the spectra. For small values of  $V_{\text{rot}}\xi$  (between 1 and 20) the radial velocity presents three levels, around 0, -1600 and -1750 km/s). For greater values of  $V_{\text{rot}}\xi$  (between 20 and 170), the level of 0 km/s disappears, while the other two levels converge to one level around -1650 km/s.

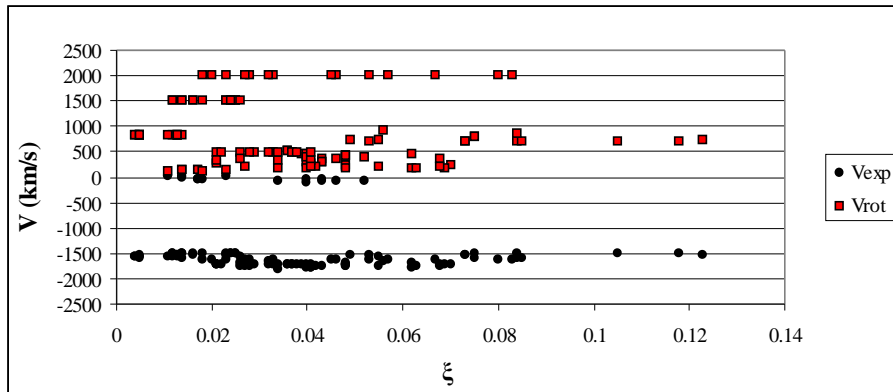


**Diagram 12:** Apparent radial ( $V_{\text{exp}}$ ) and rotation ( $V_{\text{rot}}$ ) velocities as a function of an expression of the optical depth ( $\xi$ ), for all the ions and all the spectra. For small values of  $\xi$  (between 0.004 and 0.085), there are two levels of radial velocities (around 0 and -1500 km/s) and two levels of rotation velocities (around 500 and 1700km/s). For greater values of  $\xi$  (between 0.105 and 0.123), the two levels of radial and rotation velocities consolidate to -1500 and 800 km/s respectively.

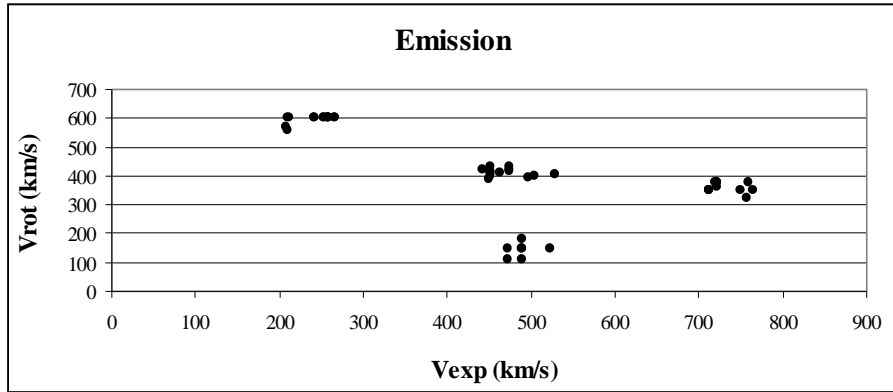


**Diagram 13:** Apparent rotation velocities ( $V_{rot}$ ) of the emitting regions as a function of the respective apparent radial velocities ( $V_{exp}$ ). When  $V_{exp}$  lies around 250 and 750 km/s,  $V_{rot}$  lies around 600 and 350 km/s respectively, while for  $V_{exp}$  around 470 km/s,  $V_{rot}$  presents two levels around 150 and 420 km/s.

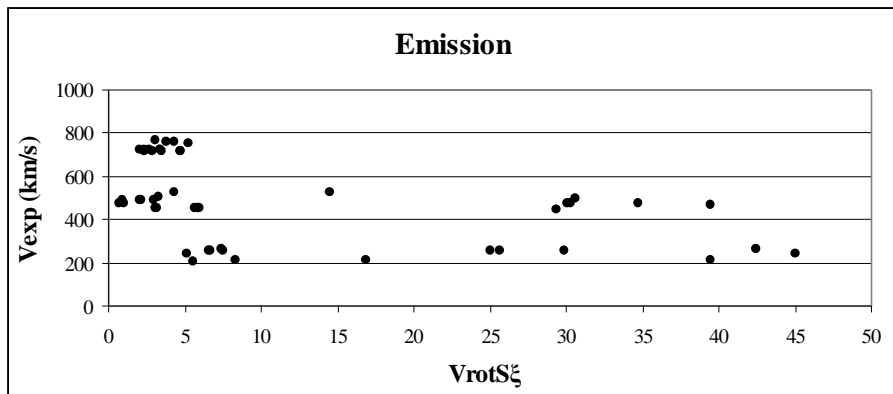


**Diagram 14:** Apparent radial velocities ( $V_{exp}$ ) as a function of an expression of the emitted energy ( $V_{rot} S_{\xi}$ ), for all the ions and all the spectra. For all the values of  $V_{rot} S_{\xi}$  (between 1 and 45) the radial velocity presents two levels, around 210 and 500 km/s. For small values of  $V_{rot} S_{\xi}$  (between 1 and 8), the radial velocity presents one more level, around 750 km/s.

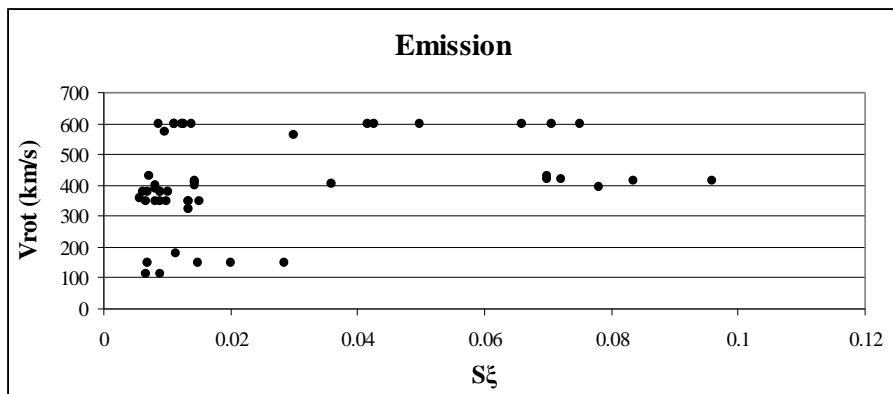


**Diagram 15:** Apparent rotation ( $V_{rot}$ ) velocities as a function of an expression of the height of the emission ( $S_{\xi}$ ), for all the ions and all the spectra. For all the values of  $S_{\xi}$  (between 0.005 and 0.100), there are two levels of rotation velocities (around 400 and 600 km/s). For small values of  $S_{\xi}$  (between 0.005 and 0.030), the rotation velocity presents one more level around 150 km/s.

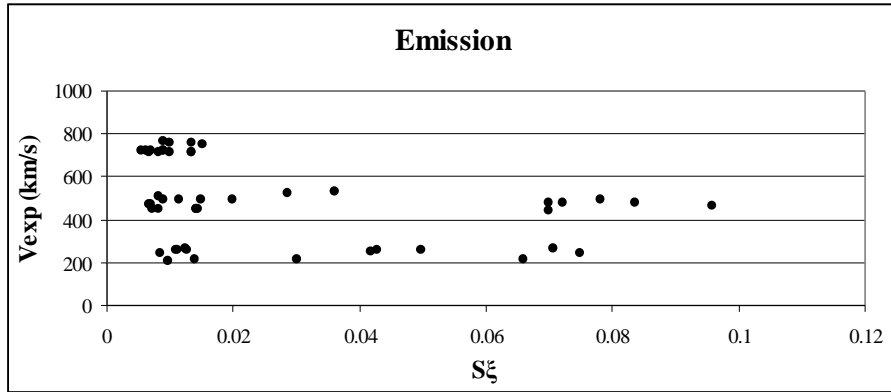


**Diagram 16:** Apparent radial ( $V_{\text{exp}}$ ) velocities as a function of an expression of the height of the emission ( $S_{\xi}$ ), for all the ions and all the spectra. For all the values of  $S_{\xi}$  (between 0.005 and 0.100), there are two levels of radial velocities (around 220 and 500 km/s). For small values of  $S_{\xi}$  (between 0.005 and 0.020), the radial velocity presents one more level around 750 km/s.

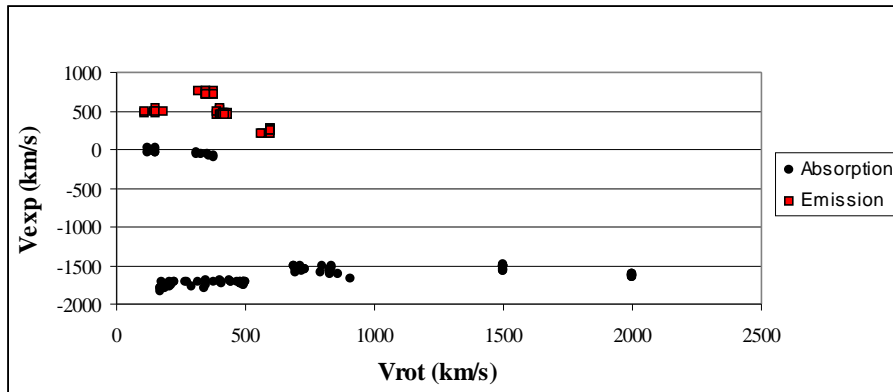


**Diagram 17:** Apparent radial velocities as a function of the respective apparent rotation velocities of the four ions, all the spectra and all the dates. The emission components present positive values of radial velocities and correspond to rotation velocities up to 600 km/s. In the case of the absorption components, when the rotation velocity lies between 120 and 500 km/s, the respective radial velocities present two levels, one around the value of 0 km/s and another around 1700 km/s. For greater values of the rotation velocity (between 690 and 2000 km/s) the respective radial velocities present only one level around 1600 km/s.

## References

- Carrasco, L., Costero, R. & Stalio, R.: 1981, A&A, 100, 183  
 Costero, R. & Stalio, R.: 1981, RMxAA, 6, 237  
 Costero, R., Doazan, V., Stalio, R. & Thomas, R. N.: 1981, emls.proc, 131  
 Danezis, E., Nikolaidis, D., Lyratzi, V., Stathopoulou, M., Theodossiou, E., Kosionidis, A., Drakopoulos, C., Christou G. & Koutsouris, P.: 2003, Ap&SS, 284, 1119  
 Franco, M. L., Stalio, R., Kontizas, E. & Kontizas, M.: 1983, A&A, 122, 9  
 Lamers, H. J. G. L. M., Gathier, R. & Snow, T. P.: 1982, ApJ, 258, 186  
 Morossi, C. & Crivellari, L.: 1980, A&AS, 41, 299